LLNL-PROC-583395

TH/5-2Ra

Multi-field two-fluid Peeling-Ballooning modes simulation with BOUT++

T. Y. Xia[1,2], X. Q. Xu[2], Z. X. Liu[1], S. C. Liu[1], B. Gui[1,2], B. Meyer[2], G. Q. Li[1] and J. G. Li[1]

[1]Institute of Plasma Physics, Chinese Academy of Sciences, Hefei, China.

[2]Lawrence Livermore National Laboratory, Livermore, CA 94550, USA

24th IAEA Fusion Energy Conference,

8-13 Oct. 2012,San Diego, USA

This work was performed under the auspices of the U.S. DoE by LLNL under Contract DE-AC52-07NA27344 and is supported by the China NSF under Contract No.10721505, the National Magnetic Confinement Fusion Science Program of China under Contracts No. 2011GB107001. LLNL-PROC-583395.

Background

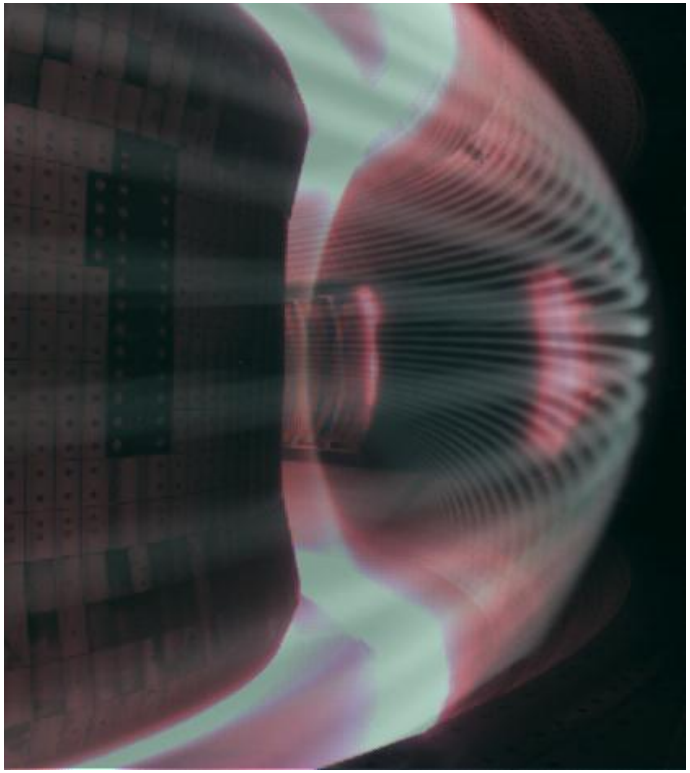

*Figure by W.H. Meyer

In H-mode, the localized edge modes (ELMs) is a dangerous perturbation for large tokamaks, such as ITER. ELMs are triggered by ideal MHD instabilities. The type I ELM is successfully explained by ideal peeling-ballooning (P-B) theory in pedestal, in which the steep pressure gradients drive ballooning mode and bootstrap current generates peeling mode.

BOUT++ simulates the Peeling-Ballooning modes through two fluid framework, which could study the nonlinear dynamics of ELMs including extensions beyond MHD physics.

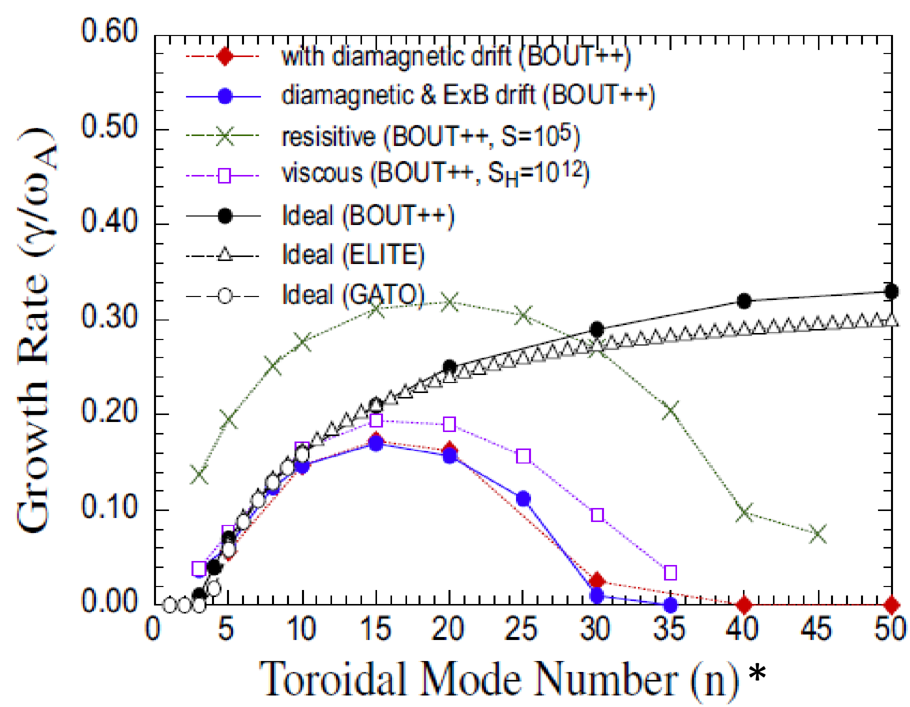

*

*Xu, X., et al., *Nucl. Fusion* 51 103040 (2011)

Setup of Toroidal Geometry

All the simulations for this work is based on the shifted circular cross-section toroidal equilibria (cbm18_dan8) generated by the TOQ code*. The equilibrium pressure is the same for all cases.

- JET-like aspect ratio
- Highly unstable to ballooning modes ($\gamma \sim 0.2\omega_A$)
- Widely used by NIMROD, M3D, M3D-C1

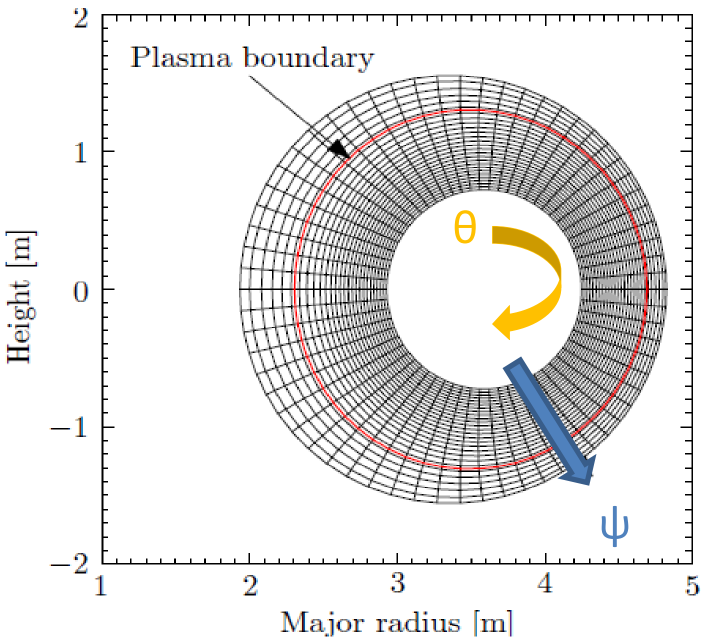

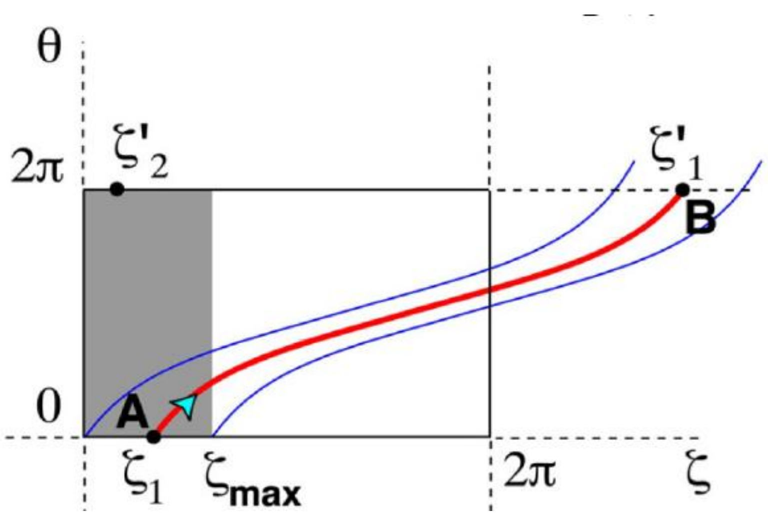

Field aligned coordinates applied in BOUT++:

$$x = \psi - \psi_0,$$
$$y = \theta,$$
$$z = \zeta - \int_{\theta_0}^{\theta} \nu(\psi,\theta) d\theta$$
$$\nu(\psi,\theta) = \frac{\vec{B} \cdot \nabla \zeta}{\vec{B} \cdot \nabla \theta}$$

*R. L. Miller and J. W. V. Dam, Nucl. Fusion 27, 2101(1987).

Multi-field two-fluid model in BOUT++

- Three-field (ϖ, P, $A_{||}$): peeling-ballooning model, without sound waves.
- Four-field (ϖ, P, $A_{||}$, $V_{||}$): sound waves are added.
- Five-field (ϖ, n_i, T_i, T_e, $A_{||}$): drift-resistive-ballooning mode, no sound waves.
- Six-field (ϖ, n_i, T_i, T_e, $A_{||}$, $V_{||}$): combine all the models together, based on Braginskii equations, the density, momentum and energy of ions and electrons are described in drift ordering[1].

[1]X. Q. Xu et al., Commun. Comput. Phys. **4**, 949 (2008).

Theoretical Equations for n_i, T_i, T_e, ϖ and ψ

$$\frac{\partial P}{\partial t} + \mathbf{V}_E \cdot \nabla P = 0$$
$$(previous\ model)$$

$$\frac{\partial n_i}{\partial t} + \mathbf{V}_E \cdot \nabla n_i = 0,$$

$$\frac{\partial T_j}{\partial t} + \mathbf{V}_E \cdot \nabla T_j = \nabla_\parallel \left(\kappa_{\parallel j} \nabla_\parallel T_j\right),$$

$$\frac{\partial}{\partial t}\varpi + \mathbf{V}_E \cdot \nabla \varpi = B_0 \mathbf{b} \cdot \nabla \frac{J_\parallel}{B_0} + 2\mathbf{b} \times \boldsymbol{\kappa} \cdot \nabla P,$$

$$\frac{\partial \psi}{\partial t} = -\frac{1}{B_0} \mathbf{b} \cdot \nabla \Phi + \frac{\eta}{\mu_0} \nabla_\perp^2 \psi - \frac{\eta_H}{\mu_0} \nabla_\perp^4 \psi,$$

Cross term
(density gradient length scale)

$$\varpi = n_{i0} \frac{m_i}{B_0} \left[\nabla_\perp^2 \phi + \frac{1}{n_{i0}} \nabla_\perp \phi \cdot \nabla_\perp n_{i0} + \frac{1}{n_{i0} Z_i e} \nabla_\perp^2 p \right],$$

$$J_\parallel = J_{\parallel 0} - \frac{1}{\mu_0} \nabla_\perp^2 (B_0 \psi),$$

$$\mathbf{V}_E = \frac{1}{B_0} (\mathbf{b}_0 \times \nabla_\perp \Phi),$$

$$P = k_B n (T_i + T_e) = P_0 + p,$$

$$\Phi = \Phi_0 + \phi.$$

We will neglect the thermal conductivities first.

$S=(\mu_0 R V_A)/\eta=10^8$

Small density gradient increases growth rate slightly in ideal MHD model, larger density quantity has stronger stabilizing effects w/ diamagnetic drifts

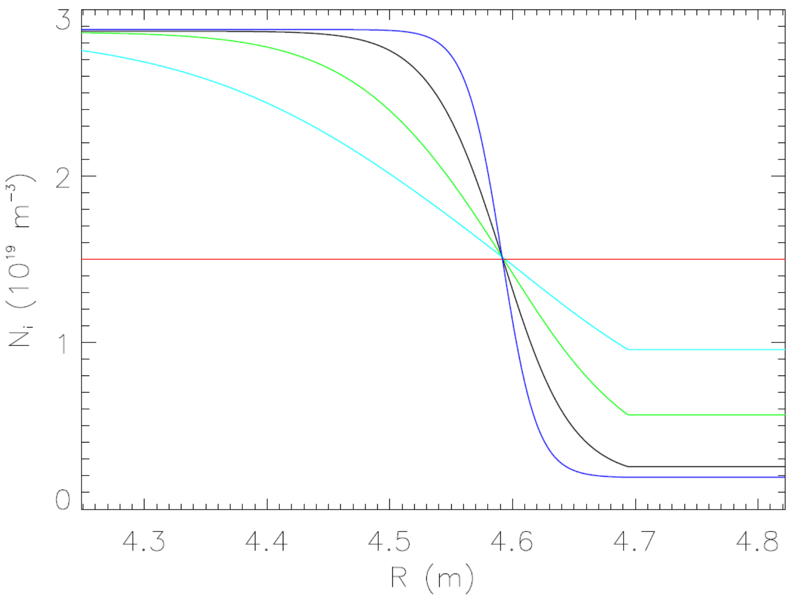

The equilibrium density profiles

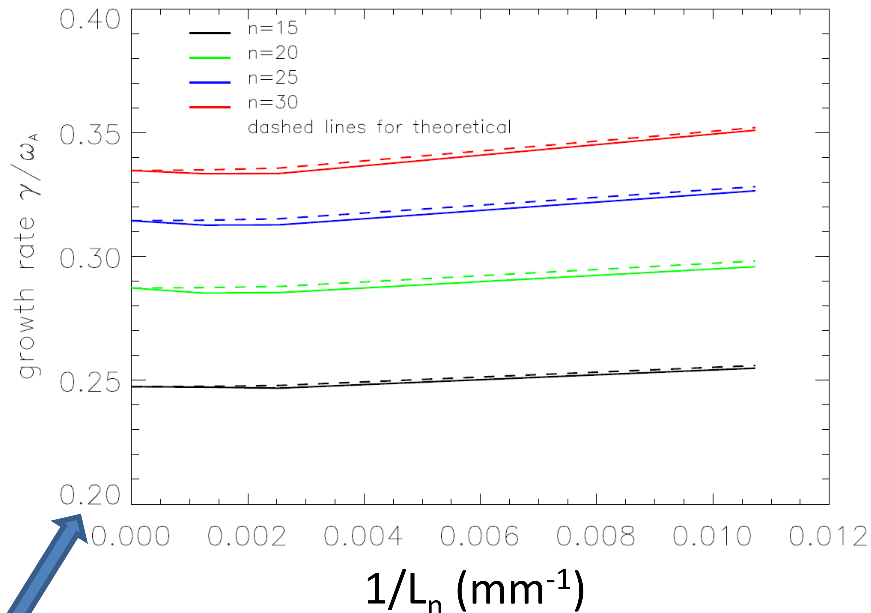

Density gradient just causes small changes for linear growth rate.

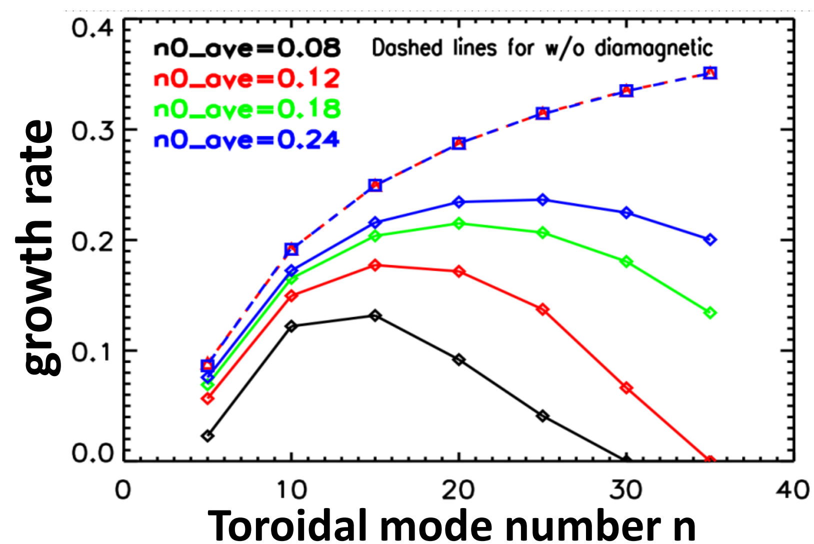

Density quantity affects linear growth rate through $\omega_* \propto 1/n_i$

Density gradient leads to large ELM size and loses the saturation behavior

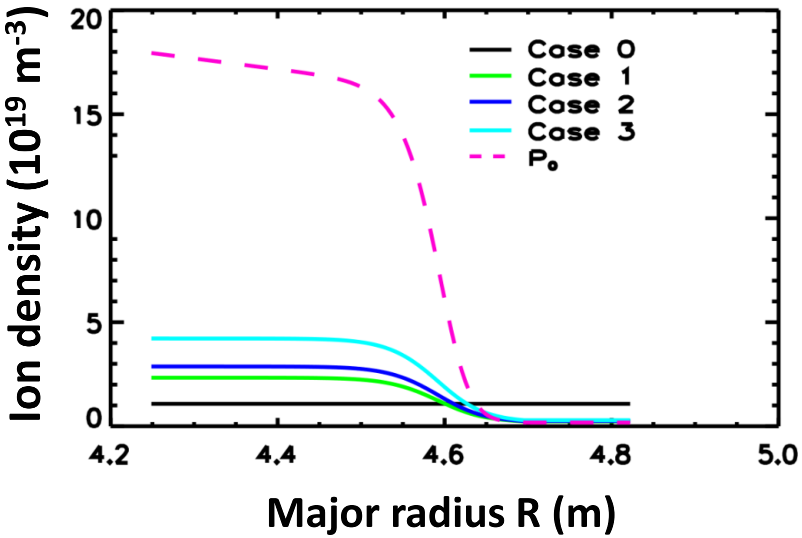

The equilibrium density profiles

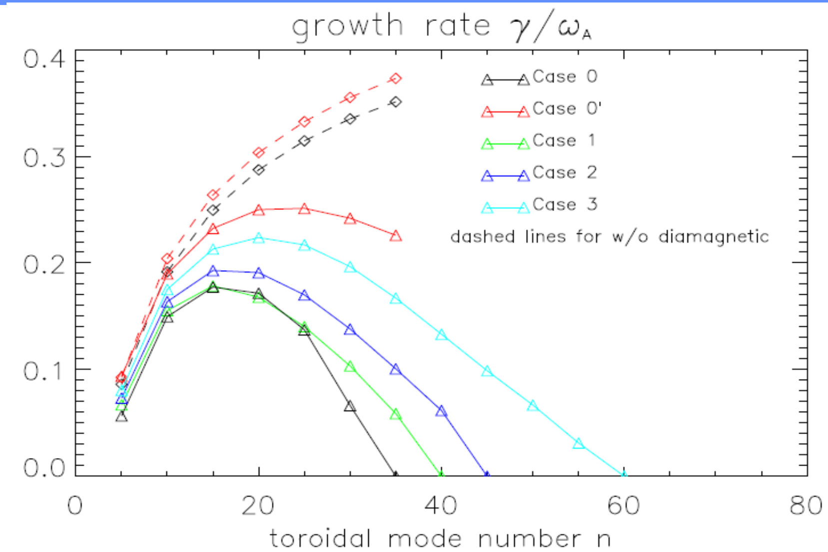

ELM size definition:

$$\Delta_{ELM}^{th} = \frac{\Delta W_{ped}}{W_{ped}} = \frac{\langle \int_{R_{in}}^{R_{out}} \oint dR d\theta (P_0 - \langle P \rangle_\zeta) \rangle_t}{\int_{R_{in}}^{R_{out}} \oint dR d\theta P_0},$$

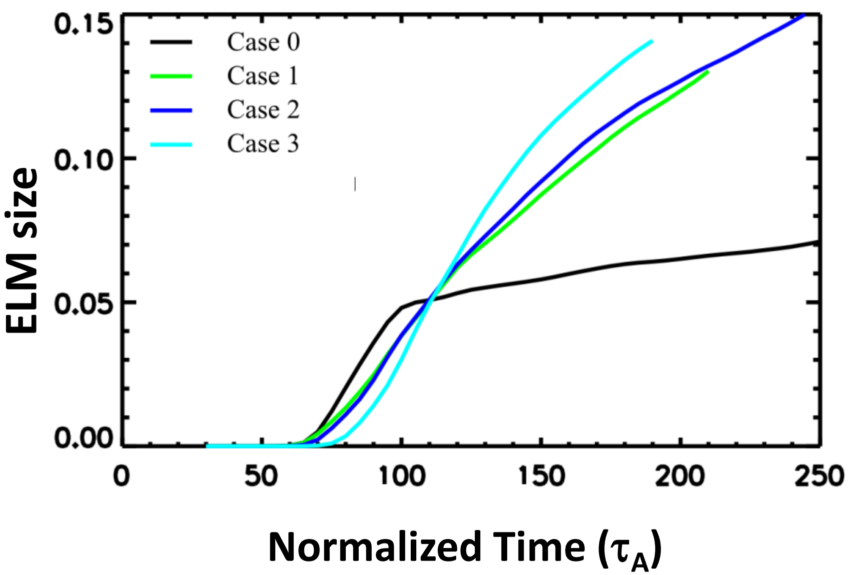

ELM size is larger for a gradient of n_0 than for the constant density case. The density gradient term provides an additional drive in the radial direction.

Radial pressure perturbations are spread by ion density gradient

Comparison of the radial pressure profiles on the outer mid-plane for the different cases for n=15.

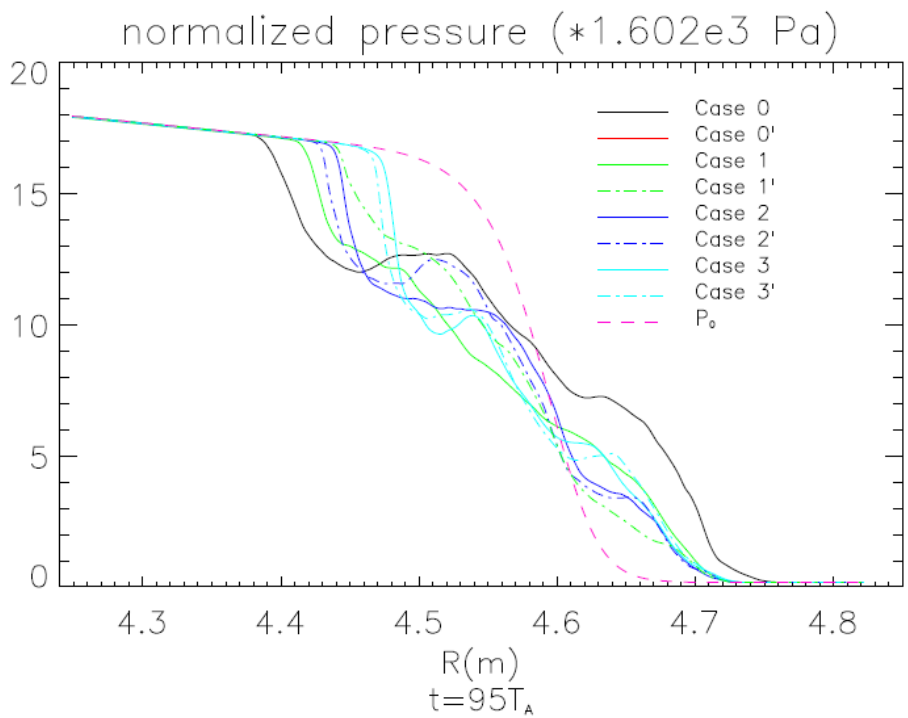

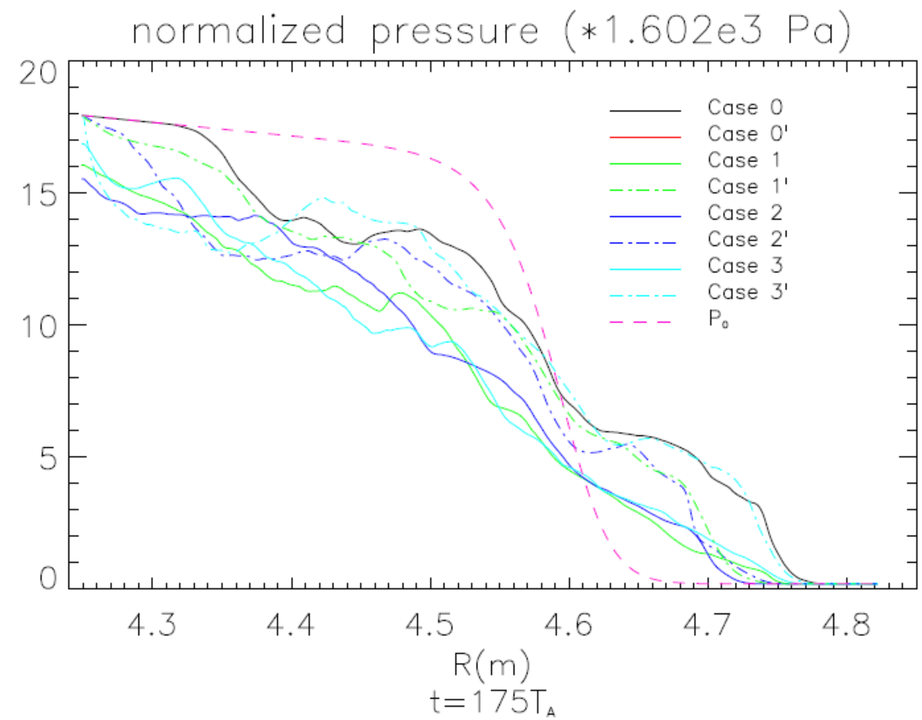

➢Case 1, 2 and 3 use Neumann BC’s in the core region and 1’, 2’ and 3’ apply Dirichlet BC’s.

➢At the early nonlinear phase. $T=95T_A$, the collapse keeps localized around the peak gradient region for all the cases. The constant n_0 case goes into the core region furthest.

➢For all nonlinear cases, except the constant n_0 case, the perturbations go into the core boundary after roughly $t=175T_A$. This is because the cross term in the vorticity equation supplies a drive in the radial direction.

Thermal conductivity and Spitzer Resistivity

➢Thermal conductivities:

$$\kappa_{\parallel i} = 3.9\frac{v_{th,i}^2}{\nu_i}$$

$$\kappa_{\parallel e} = 3.2\frac{v_{th,e}^2}{\nu_e}$$

With flux limited expressions:

$$\kappa_{fl,j} = v_{th,j}q_{95}R_0$$

Obtain the effective thermal conductivities:

$$\kappa_{\parallel j}^{e} = \left(\frac{1}{\kappa_{\parallel j}} + \frac{1}{\kappa_{fl,j}}\right)^{-1}$$

➢Spitzer resistivity:

$$\eta_{SP} = 0.51\times 1.03\times 10^{-4}\ln\Lambda T^{-\frac{3}{2}}$$

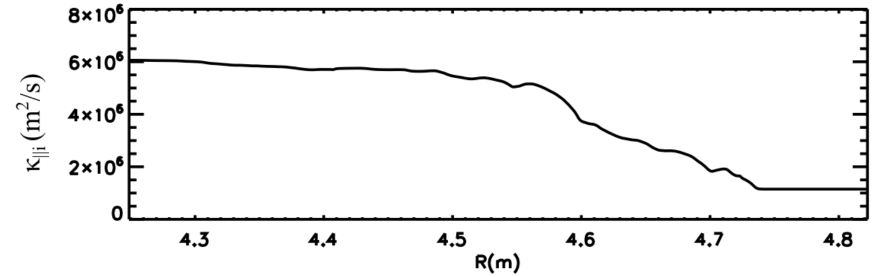

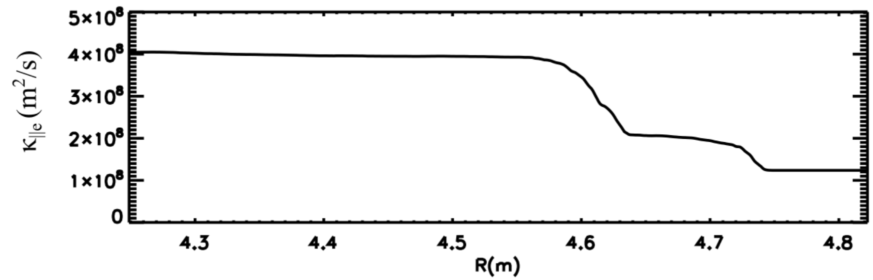

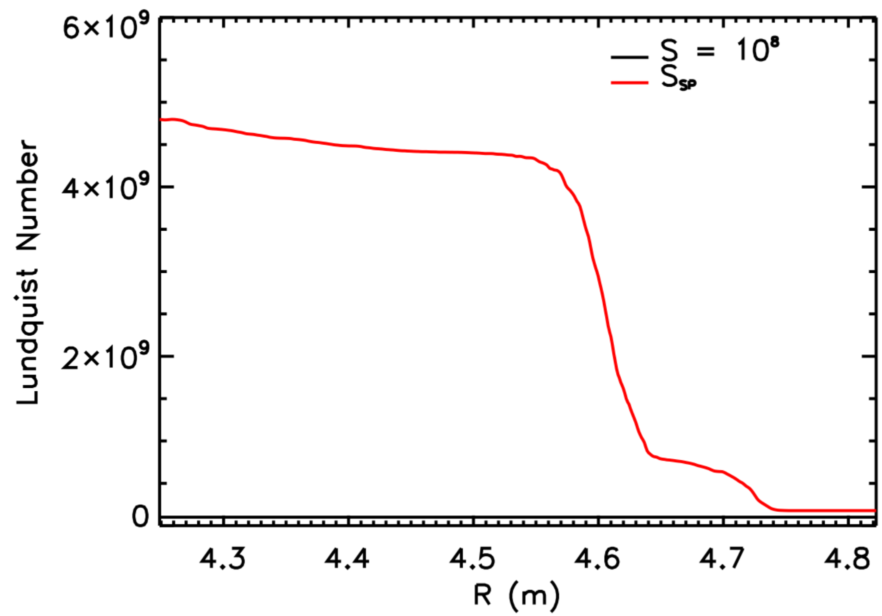

Linear effects for thermal conductivities and Spitzer resistivity

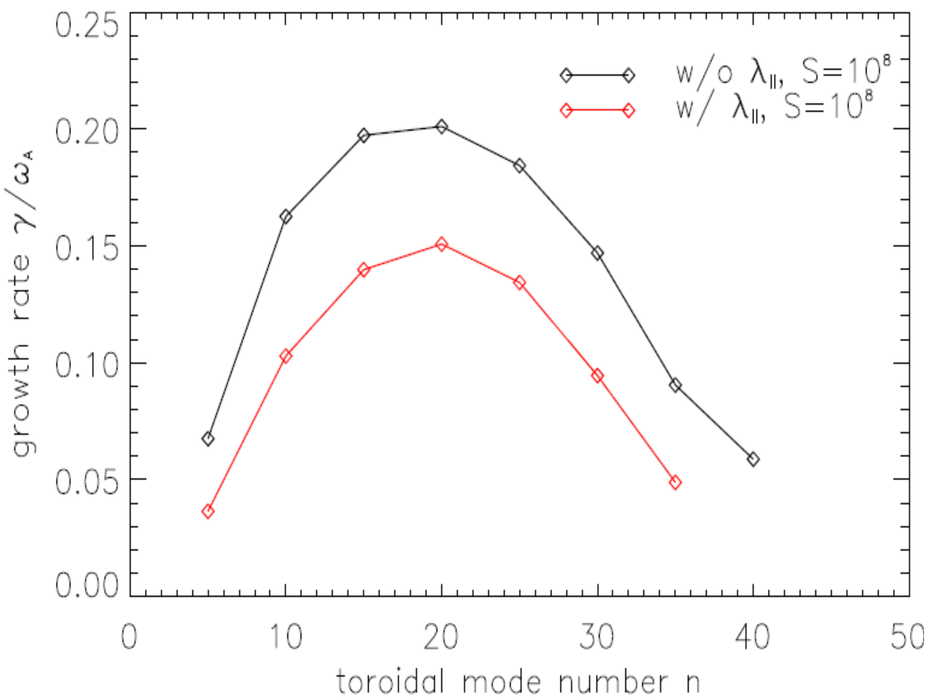

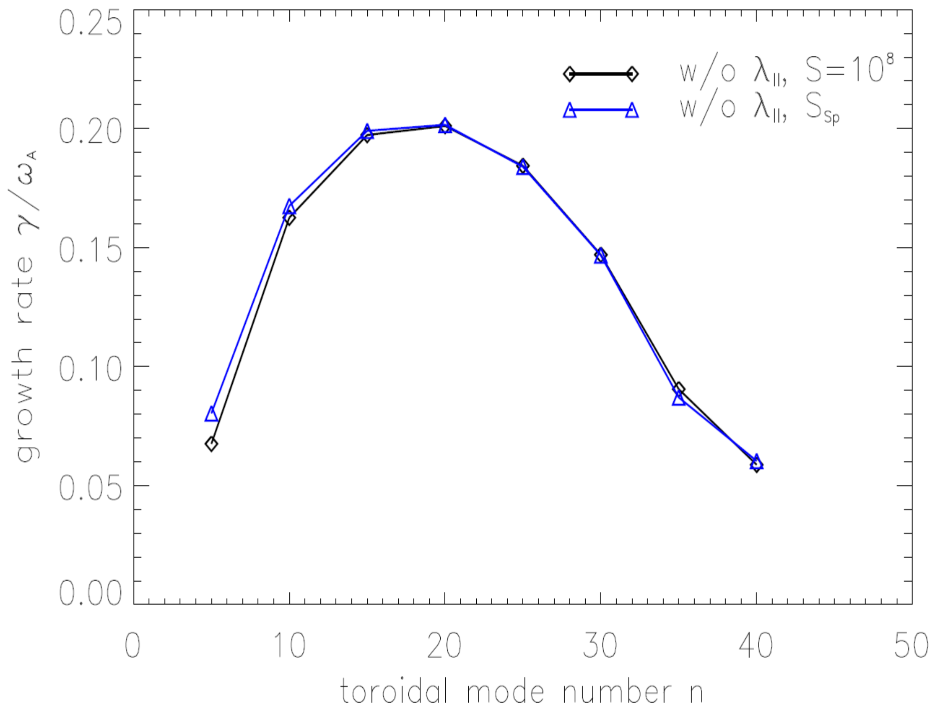

- For Case 2 with $\kappa_{||}$, the growth rates are decreased by 33.7% at least. The stabilizing effects are obvious.
- For Case 2 with S_{Sp}, the growth rates are almost the same since the equilibrium is ballooning-unstable but peeling-stable.

$K_{||}$ decreases the saturated perturbations, while η_{SP} affects little

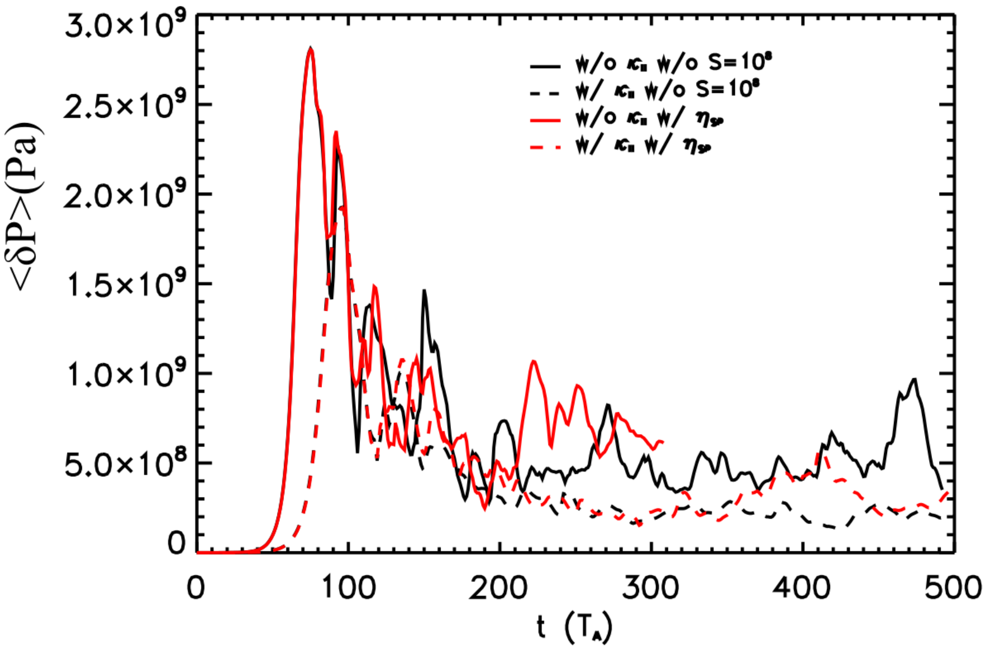

- The saturated value at nonlinear phase is decreased by thermal conductivities.
- The effects on T_e is obvious since $K_{||e}$ is much larger.

- The influence of η_{SP} is hard to be seen from the linear growth regime, because cbm18_dens8 is a strong ballooning instability and η_{SP} does not changed too much compared with S = 10^8.

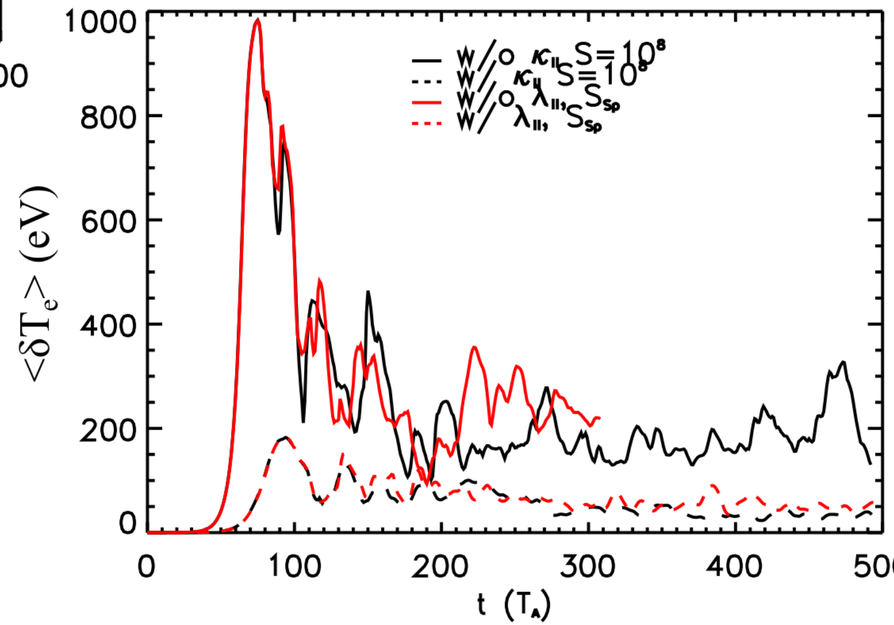

Time averaged radial profiles show transporting into the core region of the temperatures are suppressed by $K_{||}$

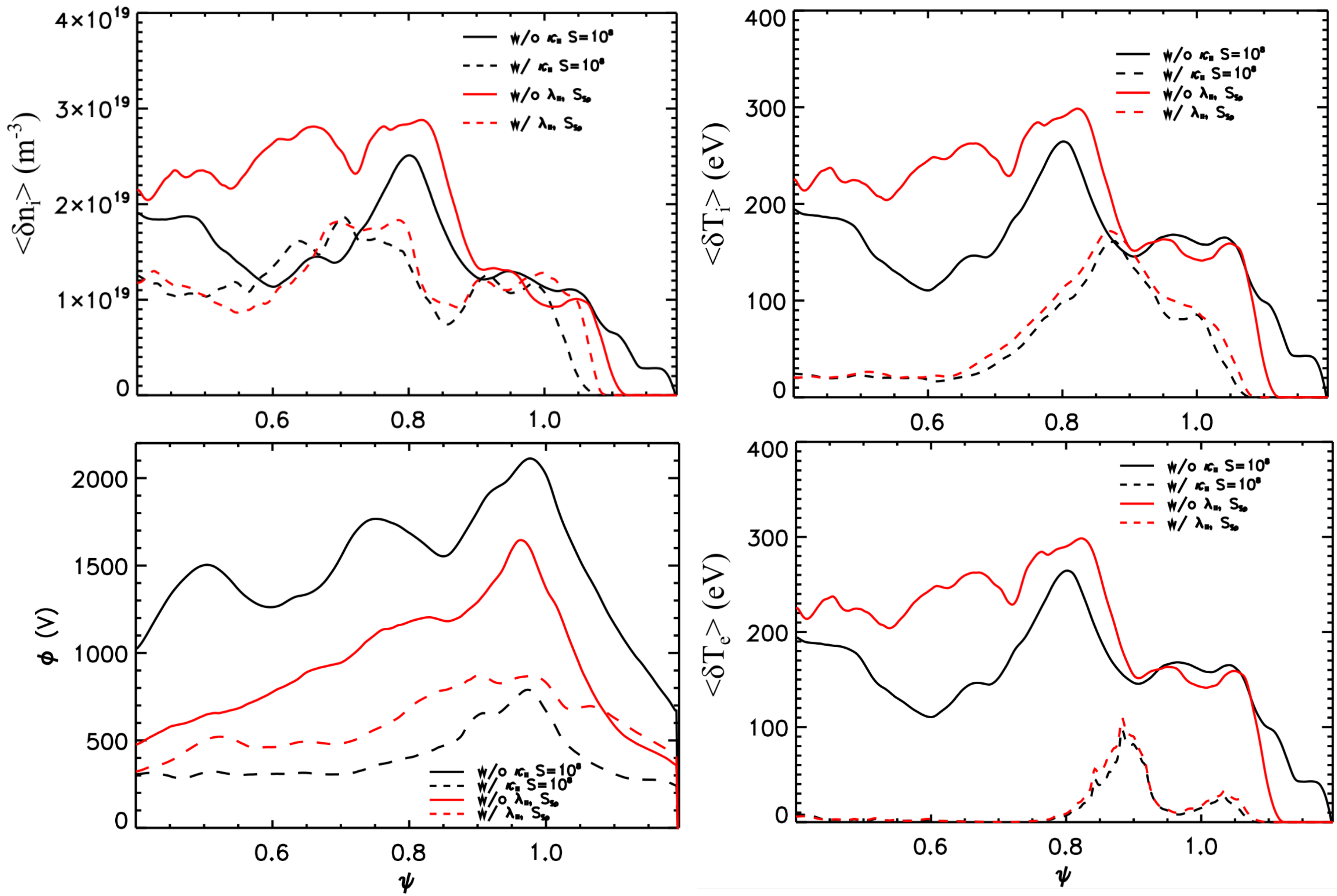

Thermal conductivities suppresses Elm size sufficiently

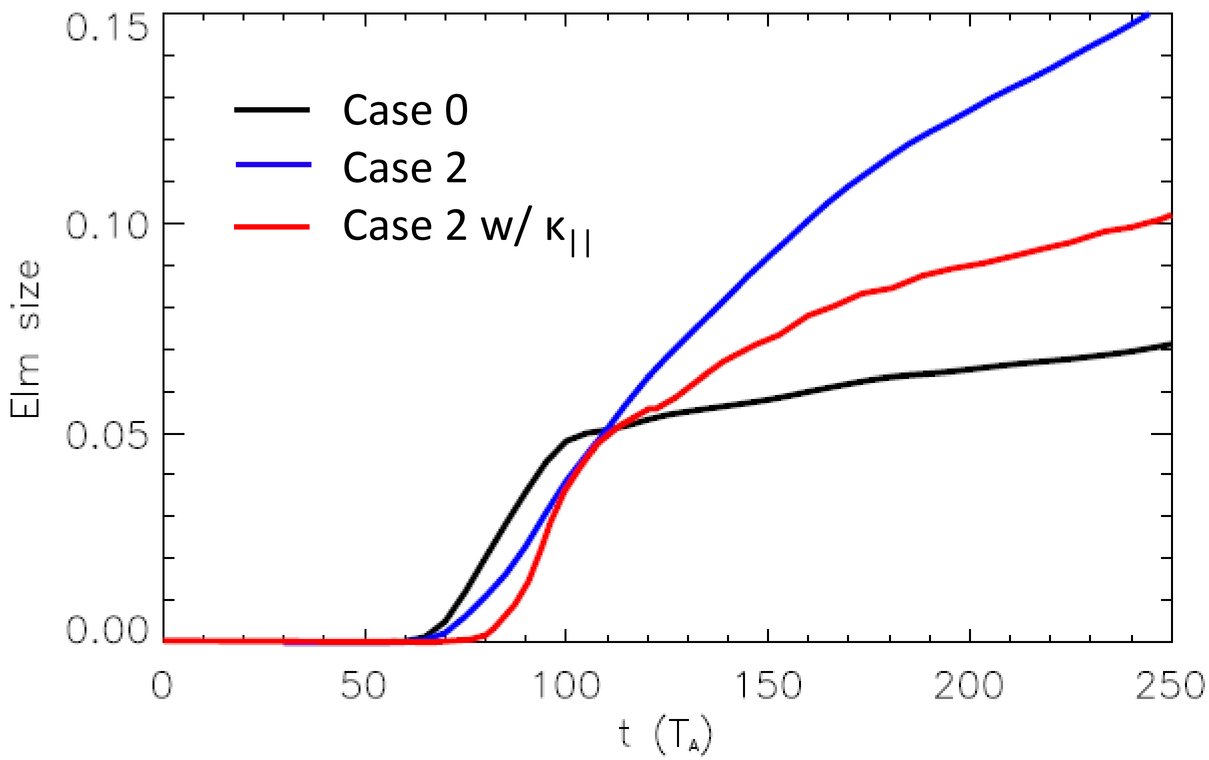

- ➢ $K_{||}$ decrease the ELM size by the ratio between 44% and 54%.
- ➢ The effects of η_{SP} are not obvious.

Theoretical Equations for 6-field 2-fluid model

Compressible terms

Parallel velocity terms

Electron Hall

Thermal force

Gyro-viscosity

Vorticity:
$$
\begin{aligned}
\frac{\partial}{\partial t}\varpi &= -\left(\frac{1}{B_0}\boldsymbol{b}\times\boldsymbol{\nabla}_\perp\Phi + V_{\parallel e}\boldsymbol{b}\right)\cdot\boldsymbol{\nabla}\varpi \\
&+B^2\nabla_\parallel\left(\frac{J_\parallel}{B}\right) + 2\boldsymbol{b}\times\boldsymbol{\kappa}\cdot\boldsymbol{\nabla}P \\
&\boxed{-\frac{1}{2\Omega_i}\left[\frac{1}{B}\boldsymbol{b}_0\times\boldsymbol{\nabla}P_i\cdot\boldsymbol{\nabla}\left(\nabla_\perp^2\Phi\right) - Z_i eB\boldsymbol{b}\times\boldsymbol{\nabla}n_i\cdot\boldsymbol{\nabla}\left(\frac{\nabla\Phi}{B}\right)^2 + Z_i eB\boldsymbol{b}\times\boldsymbol{\nabla}n_i\cdot\boldsymbol{\nabla}\left(\frac{\nabla_\parallel\Phi}{B}\right)^2\right] + \frac{1}{2\Omega_i}\left[\frac{1}{B}\boldsymbol{b}_0\times\boldsymbol{\nabla}\Phi\cdot\boldsymbol{\nabla}\left(\nabla_\perp^2 P_i\right) - \nabla_\perp^2\left(\frac{1}{B}\boldsymbol{b}_0\times\boldsymbol{\nabla}\Phi\cdot\boldsymbol{\nabla}P_i\right)\right]},
\end{aligned}
$$

Density:
$$
\begin{aligned}
\frac{\partial}{\partial t}n_i &= -\left(\frac{1}{B_0}\boldsymbol{b}\times\boldsymbol{\nabla}_\perp\Phi \boxed{+ V_{\parallel i}\boldsymbol{b}}\right)\cdot\nabla n_i \\
&\boxed{-\frac{2n_i}{B}\boldsymbol{b}\times\boldsymbol{\kappa}\cdot\boldsymbol{\nabla}_\perp\Phi - \frac{2}{Z_i eB}\boldsymbol{b}\times\boldsymbol{\kappa}\cdot\boldsymbol{\nabla}_\perp P}\boxed{- n_i B\nabla_\parallel\left(\frac{V_{\parallel i}}{B}\right)} \\
&-\boldsymbol{\nabla}\cdot\left(n_i\boldsymbol{V}_{Pi}\right).
\end{aligned}
$$

Ohm's Law:
$$
\frac{\partial}{\partial t}A_\parallel = -\nabla_\parallel\phi - \eta J_{\parallel 1}\boxed{+\frac{1}{en_e}\nabla_\parallel P_e}\boxed{+\frac{0.71k_B}{e}\nabla_\parallel T_e}.
$$

The parallel ion equation:
$$
\boxed{\frac{\partial}{\partial t}V_{\parallel i} = -\left(\frac{1}{B_0}\boldsymbol{b}\times\boldsymbol{\nabla}_\perp\Phi + V_{\parallel i}\boldsymbol{b}\right)\cdot\boldsymbol{\nabla}V_{\parallel i} - \frac{1}{m_i n_i}\boldsymbol{b}\cdot\boldsymbol{\nabla}P,}
$$

Theoretical Equations for 6-field 2-fluid model (cont.)

$$
\begin{aligned}
\frac{\partial}{\partial t}T_i \;=\;& -\left(\frac{1}{B_0}\boldsymbol{b}\times\boldsymbol{\nabla}_\perp\Phi + V_{\parallel i}\boldsymbol{b}\right)\cdot\boldsymbol{\nabla}T_i \\
& -\frac{2}{3}T_i\left[\left(\frac{2}{B}\boldsymbol{b}\times\boldsymbol{\kappa}\right)\cdot\left(\boldsymbol{\nabla}\Phi + \frac{1}{Z_i e n_i}\boldsymbol{\nabla}P_i + \frac{5}{2}\frac{k_B}{Z_i e}\boldsymbol{\nabla}T_i\right) + B\nabla_\parallel\left(\frac{V_{\parallel i}}{B}\right)\right] \\
& +\frac{2}{3n_i k_B}\nabla_\parallel\left(\kappa_{\parallel i}\nabla_\parallel T_i\right) \\
& +\frac{2m_e}{m_i}\frac{Z_i}{\tau_e}\left(T_e - T_i\right)
\end{aligned}
$$

$$
\begin{aligned}
\frac{\partial}{\partial t}T_e \;=\;& -\left(\frac{1}{B_0}\boldsymbol{b}\times\boldsymbol{\nabla}_\perp\Phi + V_{\parallel e}\boldsymbol{b}\right)\cdot\boldsymbol{\nabla}T_e \\
& -\frac{2}{3}T_e\left[\left(\frac{2}{B}\boldsymbol{b}\times\boldsymbol{\kappa}\right)\cdot\left(\boldsymbol{\nabla}\Phi - \frac{1}{e n_e}\boldsymbol{\nabla}P_e - \frac{5}{2}\frac{k_B}{e}\boldsymbol{\nabla}T_e\right) + B\nabla_\parallel\left(\frac{V_{\parallel e}}{B}\right)\right] \\
& -0.71\frac{2T_e}{3en_e}B\nabla_\parallel\left(\frac{J_\parallel}{B}\right) \\
& +\frac{2}{3n_e k_B}\nabla_\parallel\left(\kappa_{\parallel e}\nabla_\parallel T_e\right) \\
& -\frac{2m_e}{m_i}\frac{1}{\tau_e}\left(T_e - T_i\right) + \frac{2}{3n_e k_B}\eta_\parallel J_\parallel^2
\end{aligned}
$$

- Compressible terms
- Parallel velocity terms
- Electron Hall
- Thermal force
- Gyro-viscosity
- Energy exchange
- Energy flux

Peeling-Ballooning modes still dominate in 6-field model

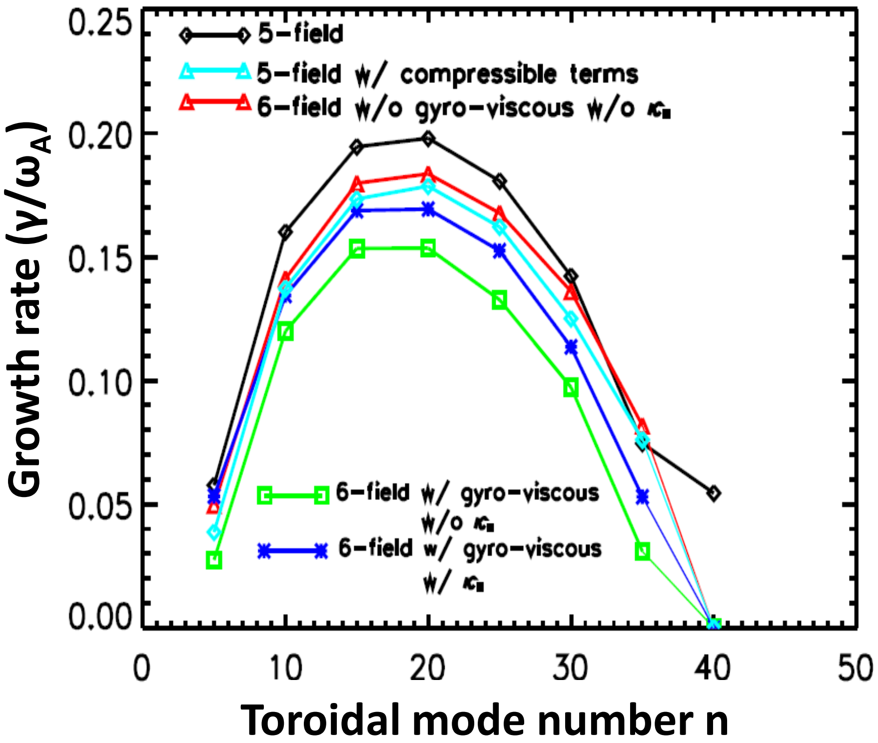

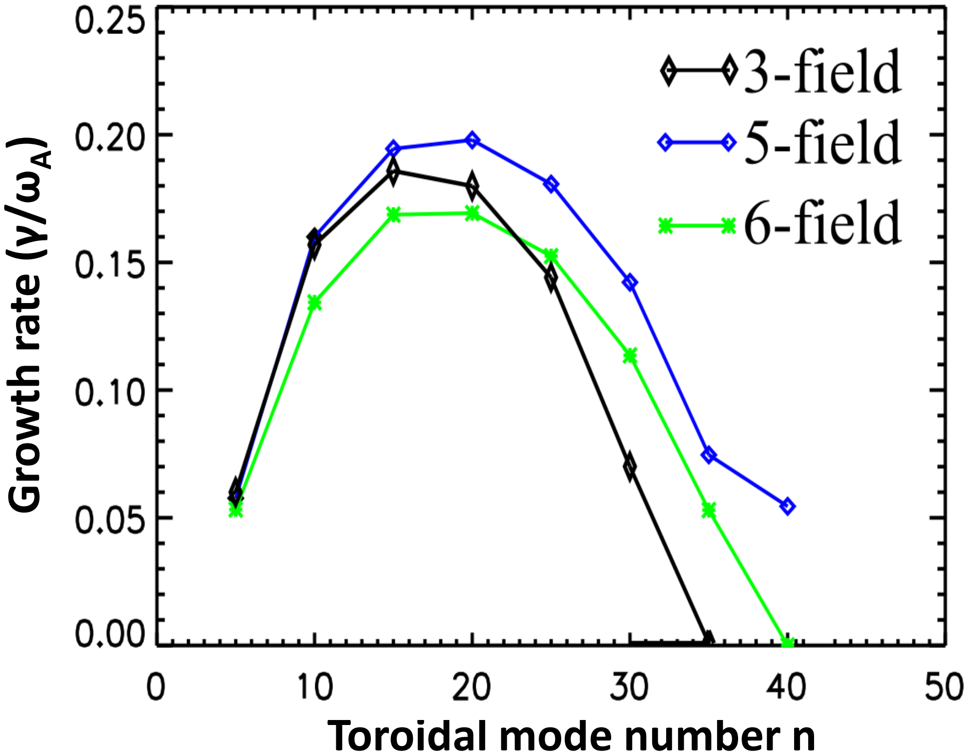

- ➢All the non-ideal physics effects decrease growth rate of 6-field by less than 25% compared with 5-field model.
- ➢3-field model is still accurate enough to simulate peeling-ballooning modes in linear phase.

6-field model get nonlinear saturation because of gyro-viscous and compressible terms

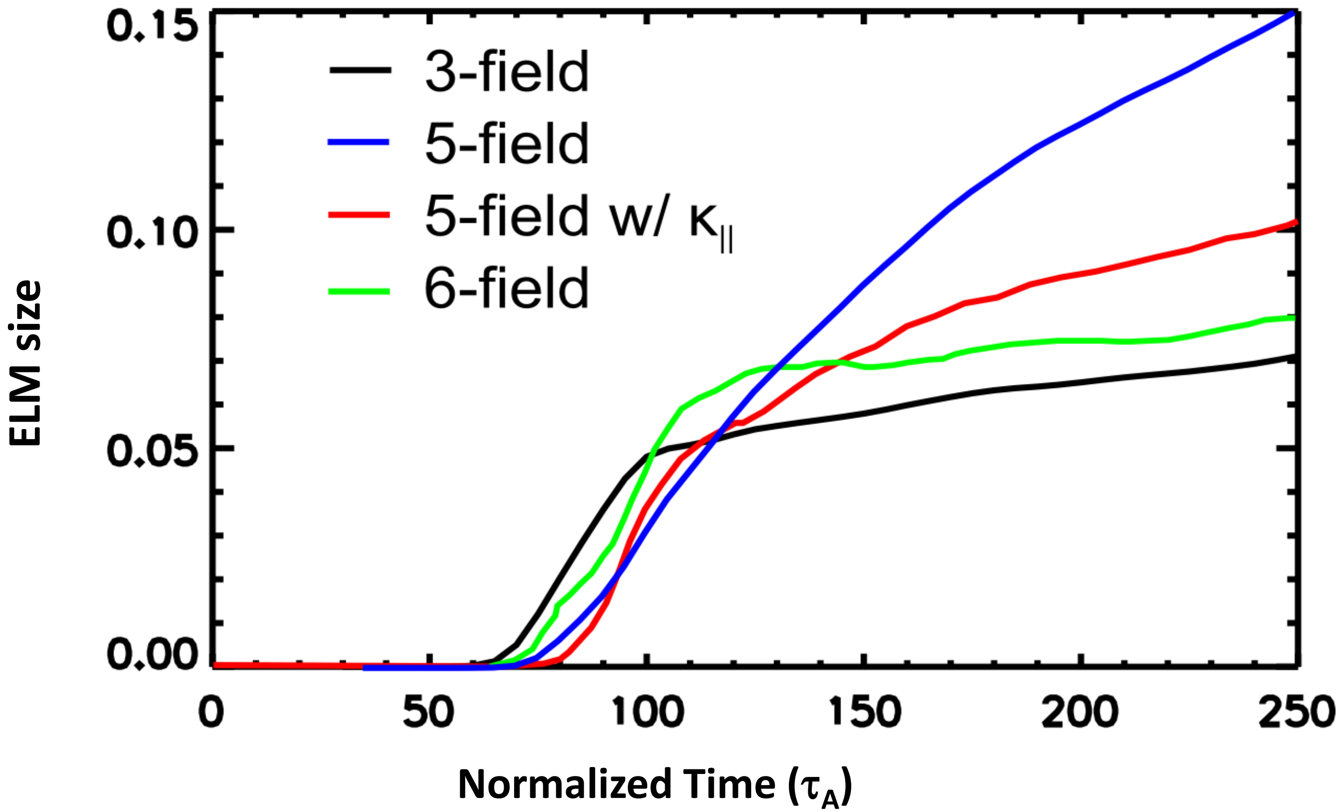

- Nonlinear Phase:
  - ✓ Vs. five-field: have saturation phase – effects of compressibility and gyro-viscosity.
  - ✓ Vs. three-field: larger ELM size – ion density gradient driven mode.

Saturation obtained after t=200T_A

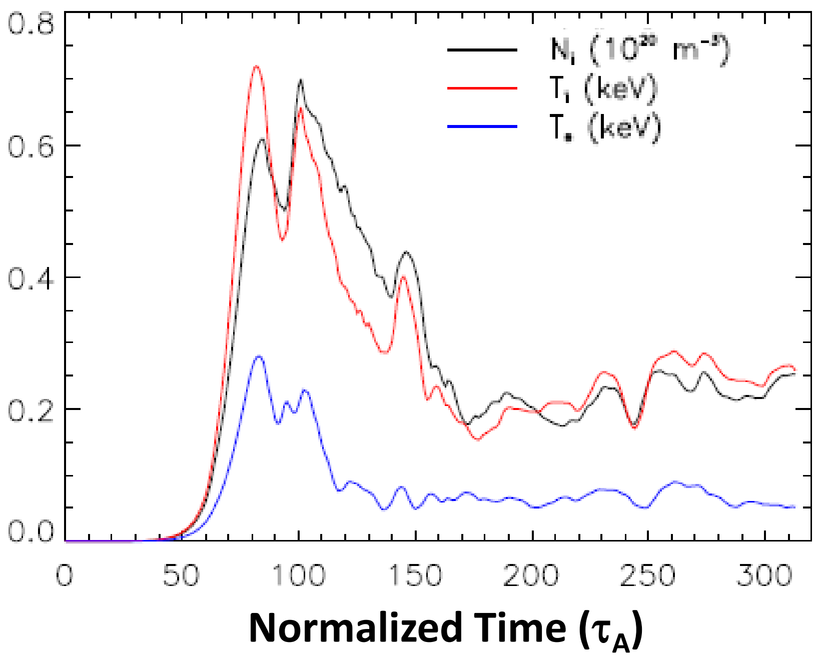

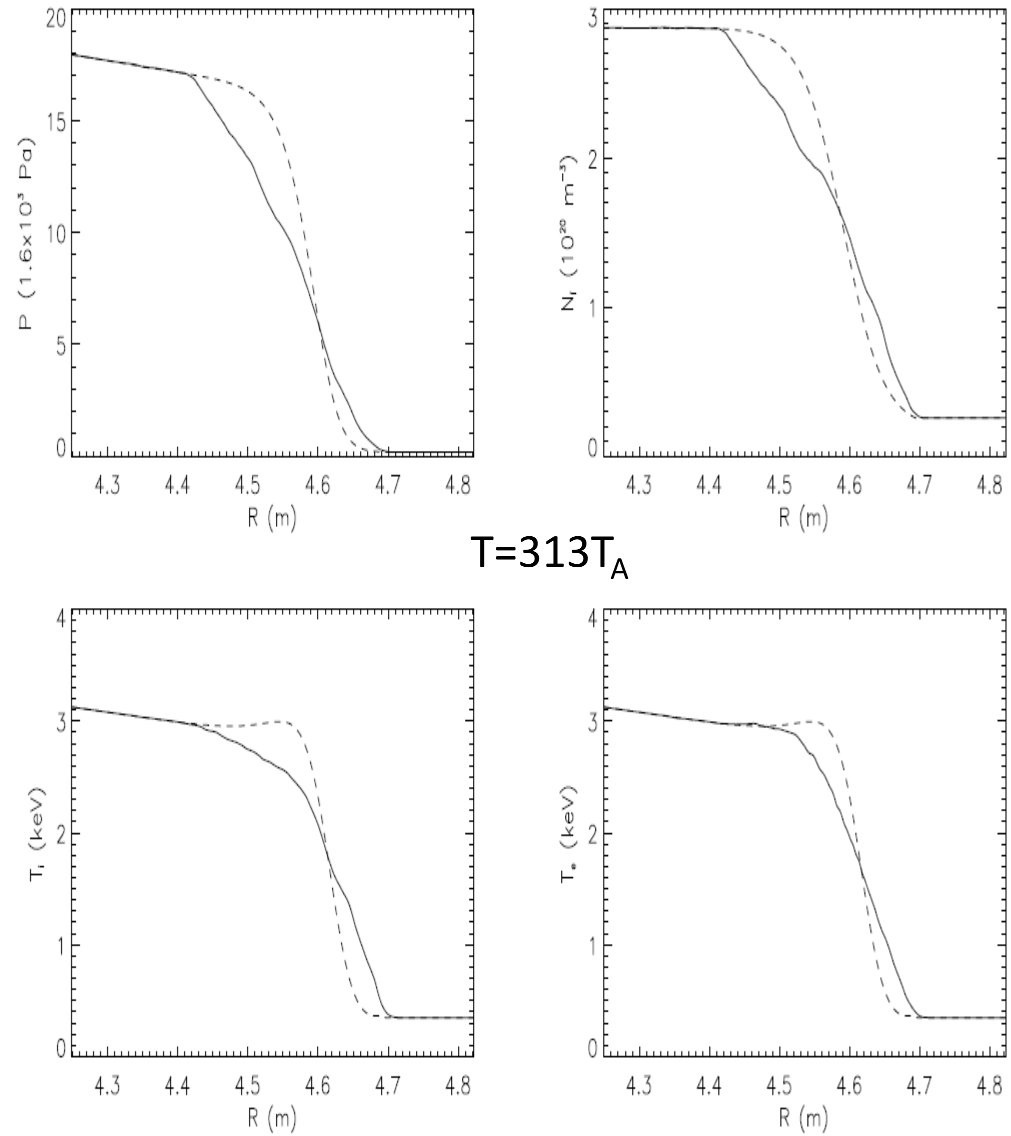

- Saturation phase are obtained after 200T_A in 6-field model.
- Perturbations are located at peak gradient region.
- After 200, L-mode are achieved.

Mode structure evolution: 6-field model get localized perturbations at peak gradient region

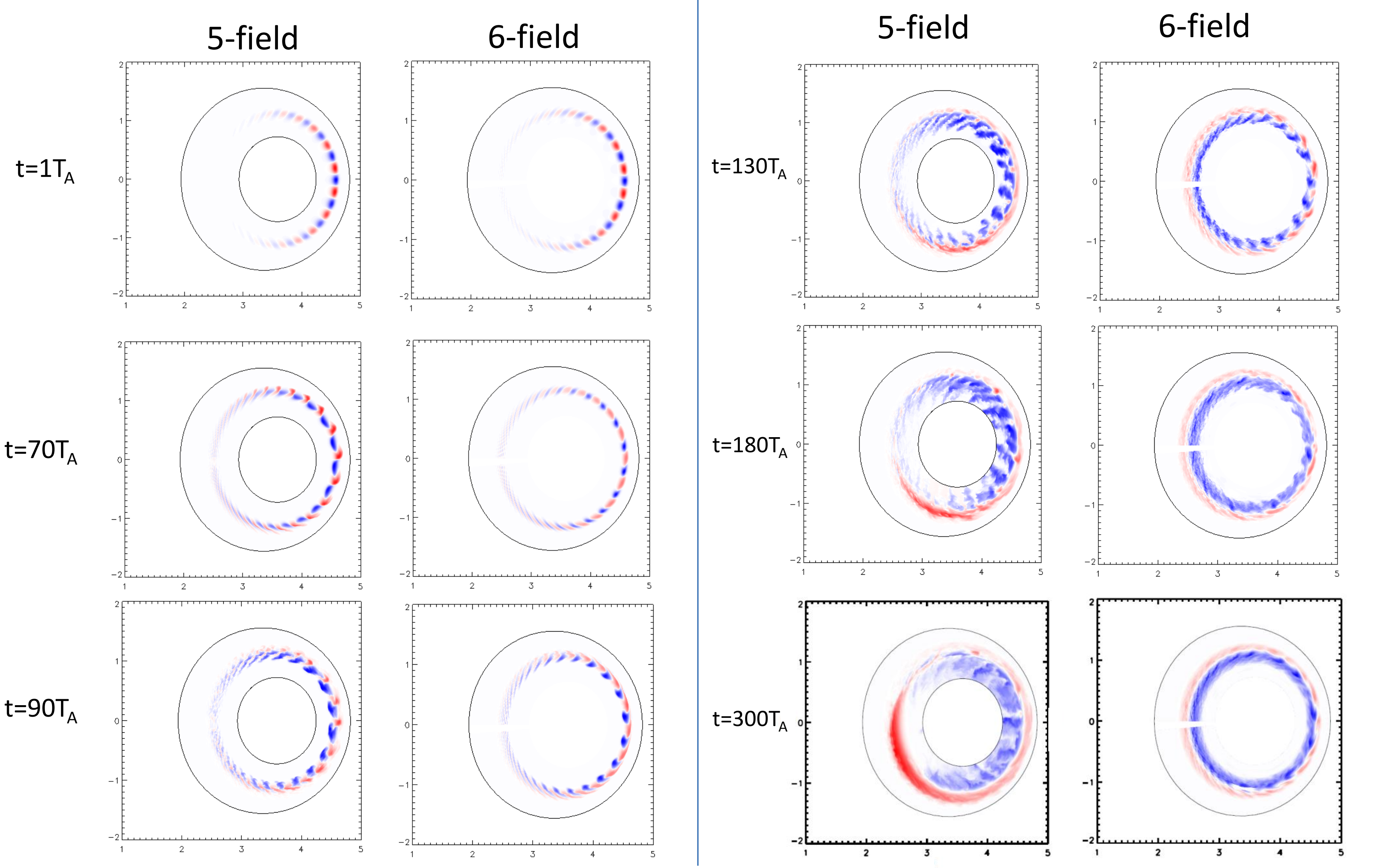

Principal Results

(1) Series of 2-fluid models are developed in BOUT++ to simulate ELM crash.

(2) Fundamental model: 3-field 2-fluid model is a good enough model for P-B stability and ELM crashes.

(3) High-n P-B mode is strongly stabilized at low density by diamagnetic drifts at low temperature.

(4) Thermal conductivities can sufficiently prevent the perturbations to propagate to the inner boundary.

(5) 6-field model is developed and it is well consistent with 3-field model.

(6) This model will be a useful tool to study energy transportation in divertor region.